

OBSERVATIONS OF THE WASP-2 SYSTEM BY THE APOSTLE PROGRAM

ANDREW C. BECKER¹, PRAVEEN KUNDURTHY¹, ERIC AGOL¹, RORY BARNES^{1,2}, BENJAMIN F. WILLIAMS¹, AMY E. ROSE¹*Draft version September 9, 2021*

ABSTRACT

We present transit observations of the WASP-2 exoplanet system by the Apache Point Survey of Transit Lightcurves of Exoplanets (APOSTLE) program. Model fitting to these data allows us to improve measurements of the hot-Jupiter exoplanet WASP-2b and its orbital parameters by a factor of ~ 2 over prior studies; we do not find evidence for transit depth variations. We do find reduced χ^2 values greater than 1.0 in the observed minus computed transit times. A sinusoidal fit to the residuals yields a timing semi-amplitude of 32 seconds and a period of 389 days. However, random rearrangements of the data provide similar quality fits, and we cannot with certainty ascribe the timing variations to mutual exoplanet interactions. This inconclusive result is consistent with the lack of incontrovertible transit timing variations (TTVs) observed in other hot-Jupiter systems. This outcome emphasizes that unique recognition of TTVs requires dense sampling of the libration cycle (e.g. continuous observations from space-based platforms). However, even in systems observed with the Kepler spacecraft, there is a noted lack of transiting companions and TTVs in hot-Jupiter systems. This result is more meaningful, and indicates that hot-Jupiter systems, while they are easily observable from the ground, do not appear to be currently configured in a manner favorable to the detection of TTVs. The future of ground-based TTV studies may reside in resolving secular trends, and/or implementation at extreme quality observing sites to minimize atmospheric red noise.

Subject headings: eclipses, stars: planetary systems, planets and satellites: fundamental parameters, individual: WASP-2b

1. INTRODUCTION

The transit technique is a highly efficient means of searching for exoplanetary systems. The detection of transiting systems requires a fortuitous observing geometry during the experiment – the exoplanet must be observed to traverse its host’s stellar disk, occurring for $\sim 10\%$ of viewing angles for hot Jupiters, but only 0.4% for Earth analogues – and a control of experimental systematics at or below the level of the transit depth. For hot-Jupiter systems around Solar-type stars, this may be as high as 1% (10^4 parts per million, ppm) of the out-of-transit depth; an Earth analogue in the same system would cause a transit depth of only 85 ppm. Ground-based observations have been able to achieve per-exposure precisions of down to 211 ppm (Tregloan-Reed & Southworth 2012) to 250 ppm (Gilliland et al. 1993) for the brightest objects. More commonly, in transit follow-up efforts where measurements of faint stars in the field is not a priority, relative photometry at the 300–500 ppm level is achieved through defocusing and precision tracking, which minimize the sampling of the flat-field function, and allow the observer to accumulate more photons before saturation (e.g. Southworth et al. 2009; Winn et al. 2009; Gillon et al. 2012; Lendl et al. 2012). Methods to model the non-random (“red”) noise in the data are also shown to improve the accuracy of photometric transit measurements (Carter & Winn 2009). However, relative precision in ground-based data is ultimately limited by atmospheric decoherence between the target and comparison

stars and across observing epochs, with leading terms including the structure function of clouds (Ivezić et al. 2007), the time-rate of change of aerosols and water vapor in the atmosphere (Stubbs et al. 2007), and atmospheric scintillation (Young et al. 1991). Space-based observations by the Kepler spacecraft (Borucki et al. 2010) set the gold-standard for relative photometry, reaching root-mean-square systematic variations of 20 ppm on timescales of several hours (Gilliland et al. 2011).

As recognized by Agol et al. (2005) and Holman & Murray (2005), the times of transits in multi-planet systems may not be exactly periodic due to mutual gravitational interactions of the planets. Multiple studies have been undertaken to search for these transit timing variations (TTVs) in known transiting exoplanet systems, using high-precision follow-up observations. The vast majority of follow-up has been undertaken on systems originally discovered from the ground, which have been heavily biased towards hot-Jupiter systems. The follow-up sampling of these transits is often irregular, due to weather, daytime, and seasonal effects. This makes detection of the libration of transit times, expected to occur over the timescales of months to years, difficult to recognize because the signal is undersampled. Boué et al. (2012) outline the difficulties in resolving TTVs in Jovian systems: they are mostly relevant for systems near (but not exactly at) mean-motion resonance, and even detected signals may yield degenerate solutions for the mass of the perturber. No unambiguous TTVs have yet been discovered in ground-based follow-up (see however Tingley et al. 2011). In contrast, the Kepler spacecraft follows-up its own discoveries through

¹ Astronomy Department, University of Washington, Seattle, WA 98195

² Virtual Planetary Laboratory, USA

continuous lightcurve coverage. Several multi-planet systems have been discovered through Kepler TTVs (e.g. Ford et al. 2012; Steffen et al. 2012a; Fabrycky et al. 2012), which have proven to be a powerful verification and mass measurement technique for planet candidates (Cochran et al. 2011).

2. APOSTLE PROGRAM

The Apache Point Survey of Transit Lightcurves of Exoplanets (APOSTLE; Kundurthy et al. 2013b) program was initiated as a systematic study of known transiting exoplanet systems on the ARC 3.5m telescope + **Agile** imager (Mukadam et al. 2011). The large aperture of the system and frame-transfer capabilities of **Agile** allow us to obtain high-precision (500 ppm RMS) relative photometry between $R = 10.8^{th}$ and $R = 10.8^{th}$ magnitude stars (XO-2; Kundurthy et al. 2013a), decreasing to 700 ppm at $R = 12.2$ vs. $R = 12.9$ (TrES-3; Kundurthy et al. 2013b), and 1000 ppm at $R = 13.8$ vs. $R = 13.6$ (GJ 1214; Kundurthy et al. 2011). Importantly, these observations happen at 100% duty cycle due to **Agile**'s frame-transfer capabilities. We make use of the **MultiTransitQuick** modeling program described in Kundurthy et al. (2013b), which uses a Markov Chain Monte Carlo (MCMC) analyzer alongside a lightcurve parameterization that minimizes degeneracies between fitted parameters, ensuring that the MCMC proceeds efficiently and faithfully samples parameter space.

This paper describes APOSTLE observations of the WASP-2 (Cameron et al. 2007) system. The host star WASP-2A is a $R = 11.3$, spectral type K1 dwarf, with an effective temperature of $T_{\text{eff}} = 5110 \pm 60$ inferred from optical and infrared colors (Maxted et al. 2011), $T_{\text{eff}} = 5150 \pm 80K$ using photospheric fitting of spectroscopic data (Triaud et al. 2010), and metallicity of $[Fe/H] = 0.08 \pm 0.08$ (Triaud et al. 2010). In our modeling we included photometric data from previous publications including Southworth et al. (2010) – who converted the timings from Cameron et al. (2007), Charbonneau et al. (2007), Hrudková et al. (2009) into the common time standard BJD(TDB) as outlined by Eastman et al. (2010) – as well as one transit epoch from Sada et al. (2012).

3. APOSTLE OBSERVATIONS OF WASP-2

The APOSTLE data reduction pipeline is described in prior publications, including our observational techniques, details of photometric extraction, detrending of the lightcurves, and parameterization of the transit model (Kundurthy et al. 2013b). Specifically to the WASP-2 system, we acquired 7 Cousins I -band and 3 r -band transit sequences between July 2007 and October 2010. The I -band images were fringe-corrected using the techniques described in Kundurthy et al. (2013a). Observations were taken with a variety of instrumental settings, starting with 0.5s observations on the nights of 2007-07-24 and 2007-07-26, and moving to longer defocused exposures starting in 2010. For the analysis here, all data were binned to equivalent-45s exposures. For all observations we used the $R = 11.4$ comparison star TYC 522-780-1.

4. MODEL FITTING

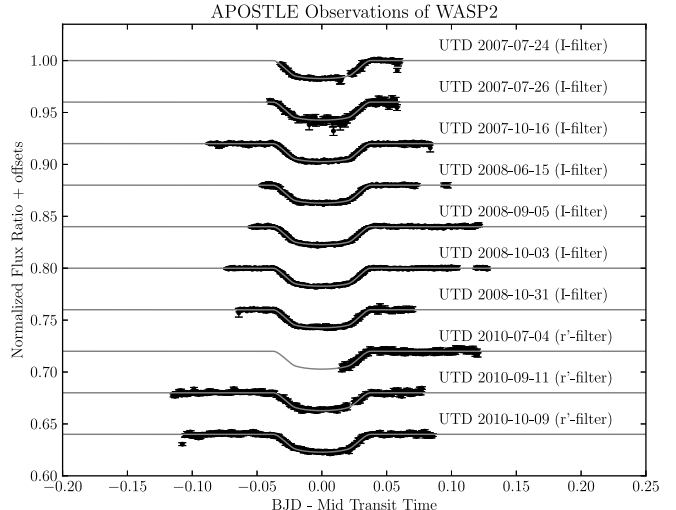


Figure 1. Seven I -band and three r -band detrended lightcurves of the WASP-2 system. The vertical axis is in normalized flux ratio units. The horizontal axis shows time from the mid-transit time in days, computed by subtracting the appropriate mid-transit time for each transit from the best-fit values in the $\theta_{\text{Multi-Depth}}$ chain.

Reduced lightcurves were detrended and modeled using the **MultiTransitQuick** (MTQ) package (Kundurthy et al. 2013b). We used MTQ in two modes: to fit for similar transit depths for data taken in a given filter (Multi-Filter model); and to fit each transit depth individually (Multi-Depth). The set of parameters used for Multi-Filter version of MTQ is $\theta_{\text{Multi-Filter}} = \{t_T, t_G, D_{j...N_F}, v_{1,j...N_F}, v_{2,j...N_F}, T_{i...N_T}\}$, where t_T is transit duration and t_G the limb-crossing duration. The per-filter fit parameters, up to the number of filters N_F , include the transit depth D , and limb darkening parameters v_1 and v_2 . Finally, the parameter set includes mid-transit times T_i up to the number of transits N_T . For the Multi-Depth version we used $\theta_{\text{Multi-Depth}} = \{t_T, t_G, D_{i...N_T}, v_{1,j...N_F}, v_{2,j...N_F}, T_{i...N_T}\}$, the main difference being we fit for each transit depth separately (N_T) instead of per-filter (N_F).

As outlined in Kundurthy et al. (2013b) and Kundurthy et al. (2013a), we did not fit for the limb darkening coefficients as they result in poorly converged Markov chains. Instead we kept them fixed at values determined using the Claret & Bloemen (2011) quadratic limb darkening models: $u_{1,I} = 0.3926$, $u_{2,I} = 0.2166$, $u_{1,r} = 0.5541$, $u_{2,r} = 0.1594$ (see Csizmadia et al. 2013, for cautions regarding this procedure). Our limb darkening terms v_1, v_2 are linear combinations of the Claret & Bloemen (2011) quadratic terms, $v_1 = u_1 + u_2$ and $v_2 = u_1 - u_2$.

Figure 1 presents our detrended data, offset for clarity, with the best-fit model lightcurves overplotted. The root-mean-square scatter about the model fits ranged from 472 ppm (2008-10-03) to 2252 ppm (2007-07-26), with a median of 626 ppm for the I -band data, and 1146 for the r -band data.

High resolution imaging of the system by Daemgen et al. (2009) reveals a faint companion within the wings of the WASP-2 host star, which will affect our conversion from D to R_p/R_* . This required that we estimate the apparent I -band and r -band magnitudes of WASP-2A and the contaminating star

(named here WASP-2/C).

We converted the reported i' and z' magnitudes from Daemgen et al. (2009) using the transformations presented in Rodgers et al. (2006) and Jordi et al. (2006), as well as on the SDSS DR7 webpage³. The final estimates yielded $r_{2A} = 11.68 \pm 0.11$, $I_{2A} = 11.00 \pm 0.11$, $r_{2C} = 17.05 \pm 0.20$, $I_{2C} = 15.39 \pm 0.20$. The two dominant uncertainties in these conversions are: the apparent brightnesses reported by Daemgen et al. (2009), which are uncertain to 0.1 magnitudes; and for WASP-2/C its redder color, which leads to a larger uncertainty in each color-term. This result indicated that 0.7% of the stellar flux in the r -band comes from WASP-2/C, and 1.7% in the I -band; the WASP-2b transit depth D increased proportionally. The change in the I -band depth was approximately four times the parameter uncertainty determined below, making this a necessary correction. The derived values of R_p/R_\star increased by 0.3% and 0.8% in the r -band and I -band, respectively.

For each parameter set ($\theta_{\text{Multi-Filter}}$ and $\theta_{\text{Multi-Depth}}$), we ran two MCMC chains, each having 2×10^6 steps. These were cropped at the beginning of the chains, where the step acceptance rate is lower than optimal (Gelman et al. 2003), yielding approximately 1.8×10^6 steps per chain used in the subsequent analysis. These chains were compared against each other to evaluate the Gelman-Rubin \hat{R} -static (Gelman & Rubin 1992) and assure that the chains sufficiently sampled model space.

Evaluation of our Multi-Depth fit indicated that the depths in the I -band were consistent at $D_I = 0.0174 \pm 0.0003$ magnitudes, while in the r -band the depth were also consistent ($D_r = 0.017 \pm 0.001$) but with a larger RMS due to having only 2 completely sampled transits⁴. We found no evidence for transit depth variations within these data, and present the Multi-Filter fits as our final results.

Fitted-for and derived Multi-Filter parameters are presented in Table 1, with the joint-probability distributions presented in Figure 2 for the fitted and derived parameters. Derived parameters include: R_p/R_\star , the radius of the planet in units of the host stellar radius; a/R_\star , the normalized semi-major axis a of the planetary orbit; the stellar density ρ_\star ; planet impact parameter b ; orbital inclination i ; and orbital period P . We found values of the Gelman-Rubin \hat{R} -static within 10^{-3} of 1.0 for all fitted parameters, indicating sufficient coverage of the chain over parameter space. The shortest effective chain length is for the time of transit on 2007-07-26 with a length of 9419. This night had some of the largest photometric uncertainties, and largest overall uncertainty on the time of transit. All other parameters have effective chain lengths larger than 10^4 , indicative of sufficient mixing in the MCMC sample (e.g. Tegmark et al. 2004). Finally, the χ^2 of the best model fit to the data is 2822.93 for 2809 degrees of freedom (reduced χ^2 of 1.005), indicating that our data (and therefore parameter) uncertainties are well understood.

5. SYSTEM PARAMETERS

Fitted-for and derived system parameters are presented in Table 1, along with their uncertainties. We note that the reported transit depths are for the WASP-2 system only, after correction for WASP-2/C. For comparison, we present the results from Southworth et al. (2010, S10), who observed in Cousins R -band. Figure 2 presents the joint probability distributions of fitted-for (*left*) and derived parameters (*right*). The left panel shows a much smaller level of correlation between parameters, making it an effective basis in which to perform MCMC. Final MTQ times of transits for each night of observation are presented in the left-hand columns of Table 2.

To model the effects of correlated lightcurve noise on our transit times, we used the Transit Analysis Package (TAP; Gazak et al. 2012), which is an implementation of the red-noise model of Carter & Winn (2009). Importantly, TAP models the amplitude of “white” (random) and “red” (correlated) noise on each night of observations. We applied TAP using the period derived from MTQ, fixed limb darkening values, and zero eccentricity and argument of periastron. For APOSTLE observations of WASP-2, the median red (white) noise contributions were 0.002 (0.0006) magnitudes in the I -band, and 0.006 (0.0006) magnitudes in the r -band. This indicated that while the statistical noise in the two datasets is comparable, the correlated noise dominates, and is larger in the r -band data. This suggests that the correlated noise comes from intrinsic stellar variability (either of the target or comparison star), or perhaps that the nights of r -band observation happened to have larger time-variation in atmospheric molecular water absorption (Stubbs et al. 2007). The TAP system parameters are included in Table 1, and times of transit in the right-hand columns of Table 2. While the TAP uncertainties are typically larger than those from MTQ, in all cases the APOSTLE analysis yields an improvement in precision over previous measurements.

5.1. Transit Timing Analysis

Using the above analysis, we found a revised ephemeris for WASP-2b of

$$P = 2.152220976 \pm 0.000000305 \text{ days}$$

$$T_0 = 2453991.5148944 \pm 0.0001232 \text{ BJD}$$

using APOSTLE results combined with Sada et al. (2012) and the non-amateur results presented in Southworth et al. (2010), for 17 epochs overall. As Figure 3 indicates, there is large scatter in the observed minus computed transit times (O-C diagram), with a reduced χ^2 of 4.7 for the TAP results (7.0 for MTQ), but it is difficult to claim a detection of coherent transit timing variations due to the sparse sampling.

To quantify the significance of this signal, we performed a 3-parameter sinusoidal fit (period in days, amplitude in seconds, and phase offset as a nuisance parameter) to the O-C data for both the TAP (and MTQ) timings. This yielded a $\Delta\chi^2$ improvement of 28.2 (47.7), with amplitudes of 32 (34) seconds and periods of 389 (437) days. We next performed 10^5 random reassignments of the timing data to the epochs of observations (i.e. we kept the APOSTLE time sampling of any putative TTV signal, but shuffled the observed amplitudes). The fitter

³ http://www.sdss.org/dr7/algorithms/jeg_photometric_eq_dr1.html

⁴ Note that these depths were determined before the corrections for WASP-2/C were applied, and thus differ from the final Multi-Filter results presented in Table 1

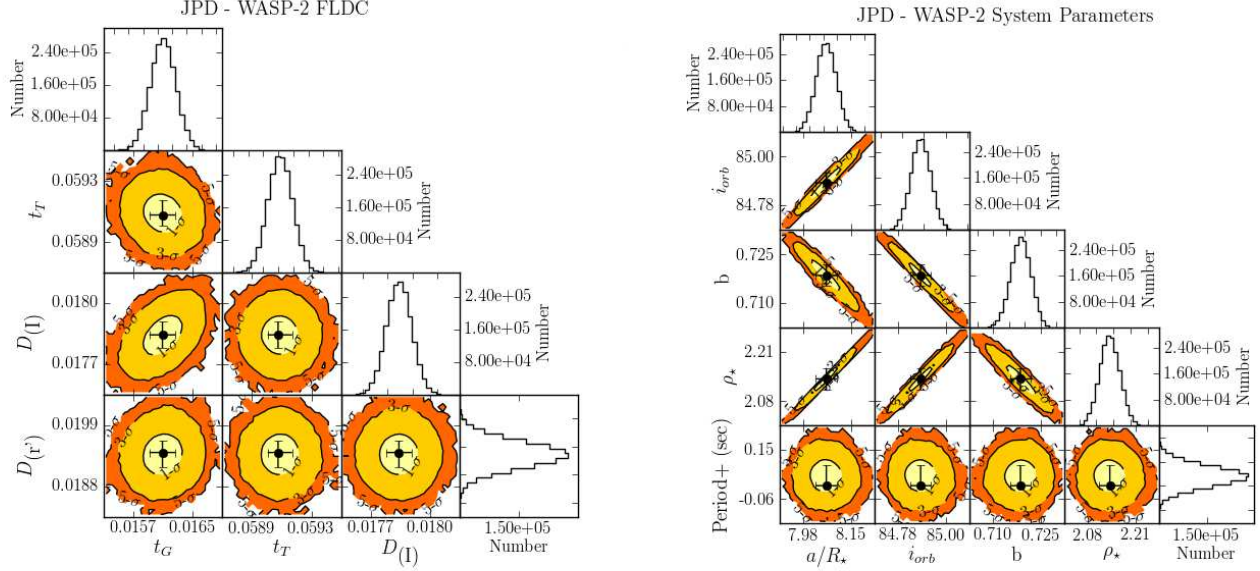


Figure 2. Plots of the joint probability distributions (JPD) of parameters from the Multi-Filter chains with fixed limb darkening. The *left* panel shows the fitted-for parameters, which are weakly correlated. The *right* panels shows the derived parameters, which tend to show larger correlations. Table 1 provides the relevant units for each parameter set.

Table 1
WASP-2 System Parameters

Parameter	Value	TAP	S10	Unit
MTQ $\theta_{\text{Multi-Filter}}$ Parameters				
t_G	0.0161 ± 0.0002	days
t_T	0.0591 ± 0.0001	days
$D(I)$	0.0178 ± 0.0001	-
$D(r')$	$0.0194^{+0.0002}_{-0.0003}$	-
$v_1(I)$	(0.6092)	-
$v_2(I)$	(0.1760)	-
$v_1(r')$	(0.7135)	-
$v_2(r')$	(0.3947)	-
Derived Parameters				
$(R_p/R_*)_{(I)}$	0.1315 ± 0.0003	0.1317 ± 0.0004	...	-
$(R_p/R_*)_{(r')}$	$0.1362^{+0.0007}_{-0.0009}$	0.1359 ± 0.001	...	-
$(R_p/R_*)_{(R)}$	0.1326 ± 0.0007	-
a/R_*	8.06 ± 0.04	7.99 ± 0.06	8.08 ± 0.12	-
ρ_*	2.14 ± 0.03	2.08 ± 0.05	2.15 ± 0.09	g/cc
b	0.719 ± 0.003	0.723 ± 0.005	...	-
i	84.89 ± 0.05	84.81 ± 0.08	84.81 ± 0.17	$^\circ(\text{deg})$
P (2.1522 days +)	1812 ± 26	...	1852 ± 34	milli-sec

was initialized to the period corresponding to the peak of the shuffled-TTV periodogram, determined using the method of Zechmeister & Kürster (2009). We then examined what fraction of these random assignments allowed a $\Delta\chi^2$ equal to or larger than that observed. This provided an estimate of the false alarm probability for any potential transit timing modulation. We found that 42% (9.7%) of the random shuffles yielded $\Delta\chi^2$ improvements at an amplitude equal to or larger than that observed. While the MTQ results were significant at the 1.7σ

level, the TAP results are more realistic given the correlated noise in our data. Thus, these data provided only marginal evidence for transit timing variations in the WASP-2 system.

6. RESULTS AND CONCLUSIONS

We presented observations and analysis of 10 transit timings of the WASP-2 system by the APOSTLE program. After an extensive treatment of the data to address and model the intrinsic systematic errors, we un-

Table 2
APOSTLE Transit Times for WASP2

Epoch	T0 (MTQ) 2,400,000+ (BJD)	σ_{T0} (BJD)	T0 (TAP) 2,400,000+ (BJD)	σ_{T0} (BJD)
146	54305.73863	0.00035	54305.73862	0.00019
147	54307.89212	0.00063	54307.89200	0.00065
185	54389.67652	0.00018	54389.67646	0.00024
298	54632.87724	0.00010	54632.87720	0.00019
336	54714.66135	0.00014	54714.66158	0.00018
349	54742.64007	0.00006	54742.64011	0.00009
362	54770.61909	0.00008	54770.61897	0.00016
646	55381.84717	0.00092	55381.84757	0.00072
678	55450.72118	0.00024	55450.72108	0.00029
691	55478.70099	0.00025	55478.70063	0.00044

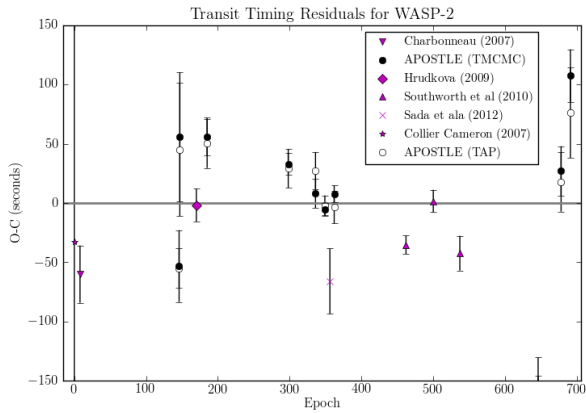


Figure 3. The observed minus computed transit times for WASP-2b. Values from APOSTLEs MTQ analysis, TAP, and previous literature are plotted. The horizontal axis represents the transit Epoch. The zero-line ephemeris is described in Section 5.1.

dertook a MCMC modeling analysis to understand the parameter uncertainties and correlations. As in previous publications, a model analysis incorporating transit duration t_T , limb-crossing duration t_G , and transit depth D yielded weakly correlated parameters (Figure 2). We corrected for a previously reported object within the photometric aperture of the WASP-2b host star (Daemgen et al. 2009) to yield the system parameters reported in Table 1. The uncertainties on these parameters are smaller than those reported in previous studies (Southworth et al. 2010). We disentangled the random and correlated noise in each lightcurve using the method of Gazak et al. (2012), and found that the red noise dominates scatter in the lightcurves, at a larger amplitude in the r -band than in the I -band.

The depths of transit coming from this analysis did not show significant time dependence. However, the times of transit shown in Figure 3 show scatter larger than the uncertainties. While a basic sinusoidal fit to this signal provided a significant improvement in χ^2 , we achieved a similar goodness of fit in 18% of random reassessments of the transit timing variations to the APOSTLE epochs. We therefore cannot conclusively report evidence of transit timing variations in the WASP-2 system.

These results mirror many of those reported in the field of ground-based transit timing measurements, where the O-C diagrams show reduced χ^2 larger than 1.0, but

there is not incontrovertible evidence of coherent transit timing librations (e.g. Eibe et al. 2012; Sada et al. 2012; Hoyer et al. 2012). A primary reason for this is sparse sampling of transit epochs, due to weather, day-time, and seasonal considerations. In contrast, the continuous observations afforded by the Kepler spacecraft provide complete sampling of the TTV signal, with both high signal-to-noise per transit and a large number of transits observed. Resolved Kepler TTVs have sufficient overall signal-to-noise to verify and weigh planets in the system. Even with tight control of experimental systematics, ground-based observations are intrinsically limited by the spatial and temporal stability of the Earth’s atmosphere; metrology at the level required to achieve calibration at the level of Kepler is currently not available.

It is likely that the lack of TTVs being detected from the ground is due to a fundamental property of the systems that are being studied. The vast majority of ground-based follow-up is focused on hot-Jupiter systems, since resolving their transit depths is achievable even with modest aperture telescopes and non-photometric observing conditions. However, as outlined by Steffen et al. (2012b), hot-Jupiter systems observed by Kepler *also* fail to show detectable TTVs, or any evidence for being in a multi-planet system. Their neighbors in exoplanet parameter space, loosely termed warm-Jupiters and hot-Neptunes, do show evidence for both TTVs and transiting companions. What this suggests is a unique dynamical pathway for the formation of contemporary hot-Jupiters, such as multi-planet scattering (e.g. Beaugé & Nesvorný 2012) leading to the ejection of lesser bodies from the system. It is thus possible that those systems that are most easily observable from the ground are also those that will fail to exhibit TTVs. Given the longevity of ground-based observing resources compared to space-based ones, it may benefit the field to undertake longer-term observations of systems to resolve secular trends such as those arising from stellar binary hosts (Ford et al. 2000) or tidal orbital decay (Hut 1981). The resolution of TTVs from the ground may also require observations from sites designed for the minimization of aerosols and water vapor, such as Llano de Chajnantor in the Atacama desert of Chile, to reduce atmospheric red noise and make resolving transits of other classes of exoplanet systems feasible.

While efforts to resolve TTVs from the ground have been largely unsuccessful, the drive to follow-up detected exoplanet systems has enabled significant leaps in the understanding and application of high-precision relative photometry. These advances are now extending to the broad application of time-domain spectroscopy during transits to map out exoplanet features in absorption (e.g. Crossfield et al. 2011), and have overall been a boon to the field of time-domain astronomy.

ACKNOWLEDGMENTS

Based on observations obtained with the Apache Point Observatory 3.5-meter telescope, which is owned and operated by the Astrophysical Research Consortium. Funding for this work came from NASA Origins grant NNX09AB32G and NSF Career grant 0645416. RB acknowledges funding from the NASA Astrobiology Institute’s Virtual Planetary Laboratory lead team, supported by NASA under cooperative agreement

NNH05ZDA001C. We would like to thank the APO Staff, APO Engineers, and R. Owen for helping the APOSTLE program with its observations and A. Mukadam for instrument characterization. We would like thank S. L. Hawley for scheduling our observations on APO. We thank N. Thomas for her help in the early analysis of the WASP-2 data. This work acknowledges the use of parts of J. Eastman's EXOFAST transit code as part of APOSTLE's transit model MTQ.

REFERENCES

- Agol, E., Steffen, J., Sari, R., & Clarkson, W. 2005, *MNRAS*, 359, 567
- Beaugé, C., & Nesvorný, D. 2012, *ApJ*, 751, 119
- Borucki, W. J., et al. 2010, *Science*, 327, 977
- Boué, G., Oshagh, M., Montalto, M., & Santos, N. C. 2012, *MNRAS*, 422, L57
- Cameron, A. C., et al. 2007, *MNRAS*, 375, 951
- Carter, J. A., & Winn, J. N. 2009, *ApJ*, 704, 51
- Charbonneau, D., Winn, J. N., Everett, M. E., Latham, D. W., Holman, M. J., Esquerdo, G. A., & O'Donovan, F. T. 2007, *ApJ*, 658, 1322
- Claret, A., & Bloemen, S. 2011, *A&A*, 529, A75
- Cochran, W. D., et al. 2011, *ApJS*, 197, 7
- Crossfield, I. J. M., Barman, T., & Hansen, B. M. S. 2011, *ApJ*, 736, 132
- Csizmadia, S., Pasternacki, T., Dreyer, C., Cabrera, J., Erikson, A., & Rauer, H. 2013, *A&A*, 549, A9
- Daemgen, S., Hormuth, F., Brandner, W., Bergfors, C., Janson, M., Hippler, S., & Henning, T. 2009, *A&A*, 498, 567
- Eastman, J., Siverd, R., & Gaudi, B. S. 2010, *PASP*, 122, 935
- Eibe, M. T., Cuesta, L., Ullán, A., Pérez-Verde, A., & Navas, J. 2012, *MNRAS*, 423, 1381
- Fabrycky, D. C., et al. 2012, *ApJ*, 750, 114
- Ford, E. B., et al. 2012, *ApJ*, 750, 113
- Ford, E. B., Kozinsky, B., & Rasio, F. A. 2000, *ApJ*, 535, 385
- Gazak, J. Z., Johnson, J. A., Tonry, J., Dragomir, D., Eastman, J., Mann, A. W., & Agol, E. 2012, *Advances in Astronomy*, 2012
- Gelman, A., Carlin, J. B., Stern, H. S., & Rubin, D. B. 2003, *Bayesian Data Analysis, Second Edition* (Chapman & Hall/CRC Texts in Statistical Science) (2 ed.) (Chapman and Hall/CRC)
- Gelman, A., & Rubin, D. 1992, *Statistical Science*, 7, 457
- Gilliland, R. L., et al. 1993, *AJ*, 106, 2441
- Gilliland, R. L., et al. 2011, *ApJS*, 197, 6
- Gillon, M., et al. 2012, *A&A*, 542, A4
- Holman, M. J., & Murray, N. W. 2005, *Science*, 307, 1288
- Hoyer, S., Rojo, P., & López-Morales, M. 2012, *ApJ*, 748, 22
- Hrudková, M., Skillen, I., Benn, C., Pollacco, D., Gibson, N., Joshi, Y., Harmanec, P., & Tulloch, S. 2009, in *IAU Symposium*, Vol. 253, IAU Symposium, 446
- Hut, P. 1981, *A&A*, 99, 126
- Ivezić, Ž., et al. 2007, *AJ*, 134, 973
- Jordi, K., Grebel, E. K., & Ammon, K. 2006, *A&A*, 460, 339
- Kundurthy, P., Agol, E., Becker, A. C., Barnes, R., Williams, B., & Mukadam, A. 2011, *ApJ*, 731, 123
- Kundurthy, P., Barnes, R., Becker, A. C., Agol, E., Williams, B., & Mukadam, A. 2013a, *ApJ*, Submitted
- Kundurthy, P., Becker, A. C., Agol, E., Barnes, R., & Williams, B. 2013b, *ApJ*, Accepted
- Lendl, M., Gillon, M., Queloz, D., Alonso, R., Fumel, A., Jehin, E., & Naef, D. 2012, *ArXiv e-prints*
- Maxted, P. F. L., Koen, C., & Smalley, B. 2011, *MNRAS*, 418, 1039
- Mukadam, A. S., Owen, R., Mannery, E., MacDonald, N., Williams, B., Stauffer, F., & Miller, C. 2011, *PASP*, 123, 1423
- Rodgers, C. T., Canterna, R., Smith, J. A., Pierce, M. J., & Tucker, D. L. 2006, *AJ*, 132, 989
- Sada, P. V., et al. 2012, *PASP*, 124, 212
- Southworth, J., et al. 2009, *MNRAS*, 396, 1023
- Southworth, J., et al. 2010, *MNRAS*, 408, 1680
- Steffen, J. H., et al. 2012a, *MNRAS*, 421, 2342
- Steffen, J. H., et al. 2012b, *Proceedings of the National Academy of Science*, 109, 7982
- Stubbs, C. W., et al. 2007, *PASP*, 119, 1163
- Tegmark, M., et al. 2004, *Phys. Rev. D*, 69, 103501
- Tingley, B., et al. 2011, *A&A*, 536, L9
- Tregloan-Reed, J., & Southworth, J. 2012, *ArXiv e-prints*
- Triard, A. H. M. J., et al. 2010, *A&A*, 524, A25
- Winn, J. N., Holman, M. J., Carter, J. A., Torres, G., Osip, D. J., & Beatty, T. 2009, *AJ*, 137, 3826
- Young, A. T., et al. 1991, *PASP*, 103, 221
- Zechmeister, M., & Kürster, M. 2009, *A&A*, 496, 577